

Diagnostics of machine tool linear axes via separation of geometric error sources

Gregory W. Vogl¹ and Michael E. Sharp¹

¹*National Institute of Standards and Technology (NIST), Gaithersburg, Maryland, 20899, USA*

*gregory.vogl@nist.gov
michael.sharp@nist.gov*

ABSTRACT

Manufacturers need automated, efficient, and robust methods to diagnose the condition of their machine tool linear axes with minimal disruptions to production. Recently, a method was developed to use data from an inertial measurement unit (IMU) to measure changes in geometric error motions. A linear axis testbed, established for verification and validation purposes, revealed that the IMU-based method was capable of measuring translational and angular deviations with acceptable test uncertainty ratios. In this study, a rail of the linear axis testbed was mechanically degraded to simulate spalling, a common degradation mechanism that can occur during machine tool operations. The rail was degraded in discrete steps from its nominal state (no degradation) to its final state (a failure state of the rail), and IMU and laser-based reference data was collected at each test stage. The contribution of geometric errors from the rail-based degradation was then separated with a technique that utilizes the various data for each run. Diagnostic metrics can then be defined for use with the IMU to facilitate industrial applications by informing the user of the magnitude and location of wear and any violations of performance tolerances.

1. INTRODUCTION

Over a machine tool's lifetime, various faults lead to performance degradation, lowering accuracy and reliability (Li, Wang, Lin & Shi, 2014). Typical sources of errors within linear axes are due to pitting, wear, corrosion, and cracks of the system components such as guideways and recirculating balls (Zhou, Mei, Zhang, Jiang & Sun, 2009). A typical machine tool has multiple linear axes, and their accuracies directly impact the quality of manufactured parts. As degradation increases, tool-to-workpiece errors increase which may eventually result in a loss of production quality

Gregory Vogl et al. This is an open-access article distributed under the terms of the Creative Commons Attribution 3.0 United States License, which permits unrestricted use, distribution, and reproduction in any medium, provided the original author and source are credited.

and/or a performance failure (Uhlmann, Geisert & Hohwieler, 2008). Yet knowledge of degradation is elusive; proper assessment of axis degradation is often a manual, time-consuming, and potentially cost-prohibitive process.

While direct methods for machine tool performance evaluation are well-established (International Organization for Standardization, 2012) and reliable for position-dependent error quantification, such measurements typically interrupt production (Khan & Chen, 2009). An online condition monitoring system for linear axes is needed to help reduce machine downtime, increase productivity and product quality, and improve knowledge about manufacturing processes (Teti, Jemielniak, O'Donnell & Dornfeld, 2010). Previous attempts at condition monitoring of linear axes had limited success, partly because of the lack of robustness and defined relationships of signals to axis degradation composed of a wide range of spatial frequencies. Consequently, efficient quantitative measures are needed to monitor the degradation of linear axes.

Recently, accelerometers have been used for dynamic metrology of machine tools (Sato & Nagaoka, 2011; Sato, Nagaoka & Sato, 2015; Smith & Hocken, 2013) and six-degree-of-freedom motion sensors exist within integrated circuit (IC) components (InvenSense Incorporated, 2016). Thus, the use of an inertial measurement unit (IMU) is attractive for on-machine condition monitoring.

Previous work has shown that one potential solution for online monitoring of linear axis degradation is the use of an IMU (Vogl, Weiss & Donmez, 2015; Vogl, Donmez & Archenti, 2016) that processes accelerometer and rate gyroscope data to detect changes in the translational and angular error motions due to axis degradation (Vogl et al., 2016). For industrial application, the IMU should be physically small and economical while satisfying measurement needs. As seen in Figure 1, a custom industrial IMU was created that is about 9.0 cm × 6.5 cm × 4.6 cm in size and contains a triaxial accelerometer and a triaxial rate gyroscope to satisfy the necessary design constraints of cost,

size, and accuracy. The bandwidths and noise properties of these sensors are shown in Table 1.

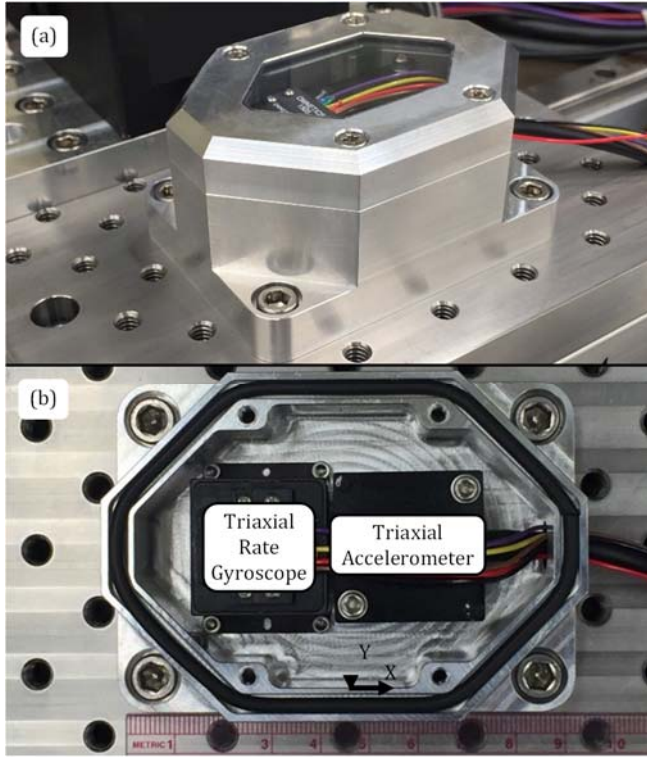


Figure 1. (a) Isometric view of industrial IMU and (b) top view of industrial IMU without its lid.

Table 1. Specified properties of sensors used in the IMU

| Sensor | Bandwidth ^a | Noise |
|----------------|------------------------|--|
| Accelerometer | 0 Hz to 500 Hz | 20 ($\mu\text{m/s}^2$)/ $\sqrt{\text{Hz}}$ |
| Rate Gyroscope | 0 Hz to 200 Hz | 35 ($\mu\text{rad/s}$)/ $\sqrt{\text{Hz}}$ |

^a frequencies correspond to half-power points, also known as 3 dB points

In this study, a rail of a linear axis was mechanically degraded from its nominal state (no degradation) to its final state (a failure state of the rail) to simulate spalling. IMU data was collected at each test stage, and an analysis technique was used to isolate the contribution of geometric errors due to the rail-based degradation. This paper outlines the experimental setup, analysis techniques, and preliminary metrics for diagnostics of rail-based degradation of linear axes. The results support the future use of IMUs for on-machine condition monitoring of linear axes within manufacturing assets.

2. EXPERIMENTAL SETUP

During operation in a machine tool, the components of a linear axis, such as rails and recirculating balls, degrade and cause the geometric performance of the axis to change. To study the ability of the IMU and accompanying diagnostics

to assess the degradation, a linear axis testbed is utilized. As seen in Figure 2, the testbed includes a linear axis system, the IMU on the carriage of the linear axis system, and a commercial laser-based system for measuring the geometric errors of the axis. While the laser-based metrology system measures the motion of the carriage with respect to the base of the linear axis, the IMU measures the changes in the inertial motion of the carriage. The laser-based system is used for verification and validation (V&V) of the IMU-based results and measures straightness and angular error motions over the travel length of 0.32 m with standard uncertainties of 0.7 μm and 3.0 μrad , respectively.

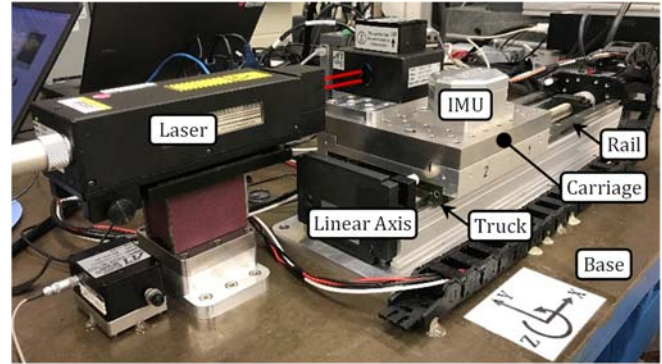


Figure 2. Linear axis testbed containing a linear axis, laser-based reference system, and IMU.

In this study, one rail of the linear axis (seen in Figure 2) was mechanically degraded to simulate spalling that can occur while a linear axis operates within machine tools. As seen in Figure 3(a), the rail has raceway grooves, upon which the recirculating balls of the trucks roll, constraining the motion of the carriage to be nominally linear. The interaction of the balls and the raceway grooves causes geometric error motions, and as the balls or the raceway grooves degrade, the geometric performance of the carriage changes.

The experiment performed involved degradation of a raceway groove, seen in Figure 3(a) prior to any mechanical degradation. To mechanically simulate spalling, a handheld grinder was used to wear the surface of the raceway groove. The length of the degradation zone was increased over the course of the experiment. Figure 3(b) to Figure 3(d) shows the progression of the ‘spalling’ on the raceway groove of the rail up to a length of 75 mm. The degradation zone length was increased incrementally by about 5.4 mm from its nominal state (no degradation, seen in Figure 3(a)) to its final state (significant degradation, seen in Figure 3(d)). Figure 4 shows the relative location and length of the degradation zone in the raceway groove for each of the fifteen (15) test stages.

Of course, the degradation is three-dimensional and not just represented by a nominal length; each degradation zone has a depth experienced by each ball of a truck. Figure 5 shows the degradation profiles measured with a 3-mm-diameter probe, typically used for coordinate measuring machines,

which was attached to a digital micrometer (with an uncertainty of $1\ \mu\text{m}$) fixed to the carriage. The probe diameter of $3\ \text{mm}$ is similar, but different from, the bearing ball nominal diameter of $3.969\ \text{mm}$. These measurements are used to corroborate and correlate the relative degradation estimations of the IMU-based results. Also, the micrometer measurements have uncertainties due to fixturing, thermal differences, etc., that are beyond the scope of this paper. One sample (Test stage 5) appears to be an outlier, likely caused by human error in fixturing. Regardless of this outlier, it appears that ‘spalling’ exists with depths greater than $50\ \mu\text{m}$ and cumulative (integral) damage linearly increasing from 0 to $\approx 58\ \mu\text{m}^2$ (depth \times length).

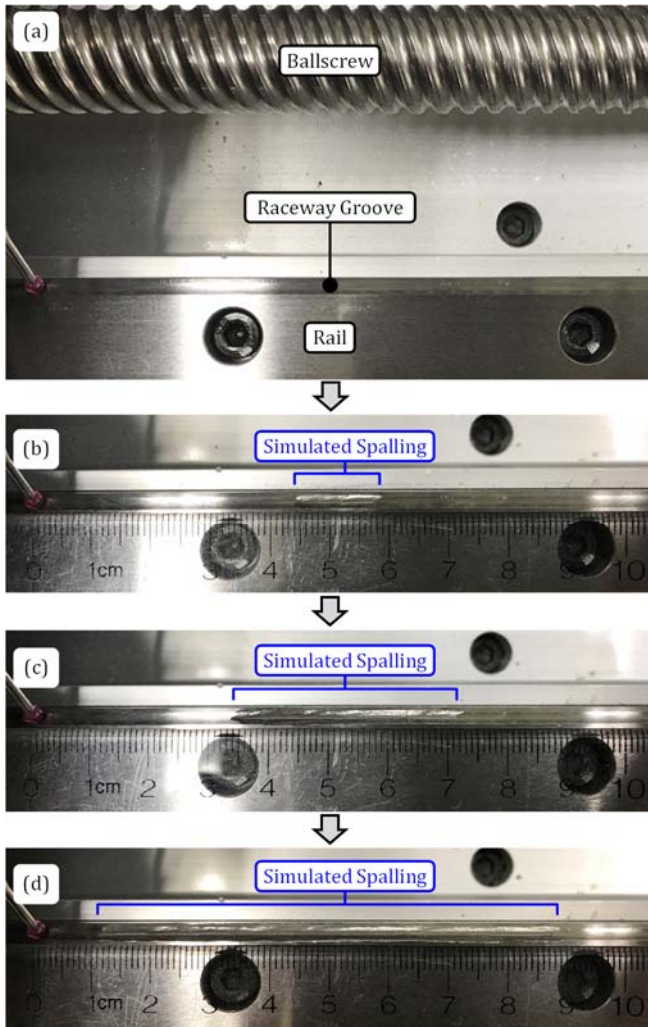


Figure 3. (a) Rail with no degradation, (b) rail with about 14 mm of ‘spalling’, (c) rail with about 37 mm of ‘spalling’, and (d) rail with about 75 mm of ‘spalling’.

Finally, for each test stage, fifty (50) runs of IMU data were collected bidirectionally at slow, moderate, and fast axis speeds (Vogl et al., 2016). Afterwards, ten (10) runs of reference data were collected bidirectionally at finite

positions of travel, specifically every 1 mm between travel positions 1 mm and 321 mm. The IMU data (accelerometer and rate gyroscope data) for each run was processed according to the IMU-based method to yield the 6-degree-of-freedom error motions (Vogl et al., 2016): one positioning error motion, two straightness error motions, and three angular error motions. Thus, six error motions are associated with each of fifty runs for all fifteen stages. These error motions were used for physics-based diagnostics described in the following sections.

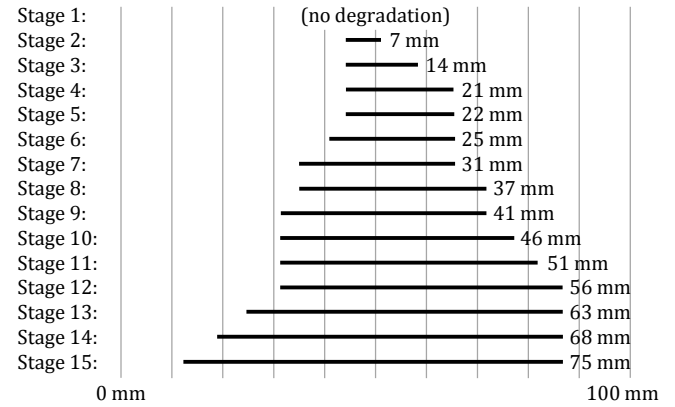


Figure 4. Schematic of relative location and length of degradation zone in raceway groove for each stage.

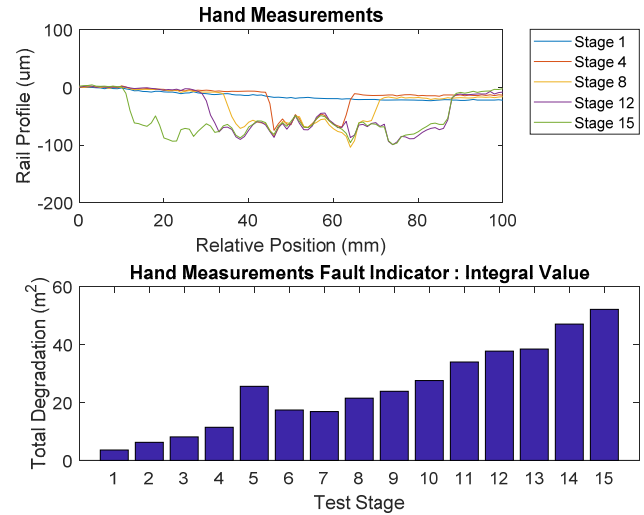


Figure 5. Degradation profiles of the rail raceway groove for certain test stages.

3. CONTRIBUTORS TO MEASURED ERROR MOTIONS

The IMU-based method should ultimately be used for diagnostics, prognostics, and health management of linear axes within production machines. Achieving these goals relies on using the IMU data to detect changes in error motions and determine the causes of these changes through diagnostic methods. However, the development of a root-

cause analysis first requires an understanding of the general types of error sources and their effects on the error motions.

Table 2 shows the physical sources of error motions in linear axes and the main errors affected by these physical sources. As seen in Table 2, the trucks and rails affect mainly the two straightness error motions and the three angular error motions, while the other components (lead screw, ball nut, and controlled motor) move the carriage and affect mainly the one positioning error motion. Technically, all components affect all error motions, but Table 2 focuses on the significant relationships between sources and error motions for root-cause diagnostics.

Table 2. Error sources and error motions in typical linear axis

| Error Source | Main Error Motions Affected by Source | | |
|------------------|---------------------------------------|--------------|---------|
| | Positioning | Straightness | Angular |
| Truck | — | Yes | Yes |
| Rail | — | Yes | Yes |
| Lead Screw | Yes | — | — |
| Ball Nut | Yes | — | — |
| Controlled Motor | Yes | — | — |

Each error motion of Table 2 can be decomposed into its constituent parts, as outlined in Table 3, which shows the types of error motions caused by each physical error source. In general, each error motion is composed of repeatable and non-repeatable terms. The non-repeatable terms simply do not repeat from run to run among collected IMU data. The repeatable components, on the other hand, are repeatable from run to run but are of one of two natures: ‘phase-fixed’ or ‘phase-shifted’. The ‘phase-fixed repeatable’ terms are fixed functions of carriage position, but the ‘phase-shifted repeatable’ terms shift their phases as functions of carriage position from run to run. For example, as seen in Table 3, a rail yields phase-fixed repeatable error motions because the rail is fixed in space, while a truck yields phase-shifted repeatable error motions because the balls in the truck recirculate in a way that causes the balls to ‘shift’ in phase relative to the rail from run to run.

Table 3. Error motion types in typical linear axis

| Error Source | Error Motion Type | | |
|------------------|------------------------|--------------------------|----------------|
| | Phase-Fixed Repeatable | Phase-Shifted Repeatable | Non-Repeatable |
| Truck | — | Yes | Yes |
| Rail | Yes | — | Yes |
| Lead Screw | Yes | — | Yes |
| Ball Nut | — | Yes | Yes |
| Controlled Motor | Yes | — | Yes |

The question remains: How do we separate the error terms outlined in Table 3 for each of the error motions outlined in Table 2? Answering this question relies on the development of a comprehensive root-cause analysis, which is beyond the

scope of this paper. In contrast, the work described herein focuses only on determining and diagnosing the rail-based errors. The ‘phase-fixed repeatable’ rail-based error motions are first separated from all other errors via the technique outlined in the next section, then diagnostics are performed on these error motion components to track rail degradation.

4. METHOD TO DIAGNOSE RAIL-BASED CHANGES IN ERROR MOTIONS

After collecting a total of 50 individual runs for the IMU data and 10 runs for the laser-based reference data, a converged value for each point along the rail path needed to be created from these individual passes. This operation serves to remove noise (part of the non-repeatable errors referenced in Table 3) and decrease the uncertainty associated with the individual runs by creating a higher fidelity map of the displacement at each point along the rail. The simplest method for combining the 50 individual runs would be to take a truncated mean of the concurrent position data, excluding the extrema values as outliers. However, for this work, it has been found that the high variation of the IMU signal low-frequency components between collection instances obfuscates small-scale degradation isolation. This variance is likely due to sensor noise and natural variations in the absolute position and orientation of the rail and IMU due to temperature and other external effects.

To help reduce the effects of the low-frequency noise on the final resulting metric, a high-pass median filter is applied to the data prior to combining. The width of this filter is determined as half the length of the rail (≈ 0.15 m). Mandating the largest window allows the capture of the lowest frequency data possible, while still removing the base deflection of the rail.

By using this form of high-pass filtering, environmental effects (such as slight warping from temperature change) and benign changes in setup can be efficiently filtered out of the resulting analysis. The basic assumption allowing this is that detrimental degradation will occur in localized areas rather than to the overall rail. Pitting or spalling are examples of degradation attuned to this form of degradation monitoring. Full beam shifting or relative torqueing respective to the opposing rail could also be monitored for via static baseline monitoring or concurrent change monitoring between the rails. These are not a focus of this paper, but may be addressed in future work.

Once an accurate estimation of the true underlying deflection path of the rail for each test stage is created, the next step is to map the change of the path deflection over time. The deflection path of the earliest test path (zero degradation) is established as the prototype baseline to quantify these changes by comparing it to all subsequent tests paths.

After the point-by-point residuals are determined for each query path, the final step is to calculate the analytic amplitude

of these values via the Hilbert transform. This allows for better trending with algorithms set to monitor the integral of the total degradation across the rail.

5. RESULTS

Both the IMU data and data taken from the laser-based reference system are processed and evaluated in the exact same way to allow for direct comparisons between the results. An example of the raw data for the vertical (Z) direction collected during a single testing cycle is shown in Figure 6. This is a direction expected to be affected by the induced spalling of this experiment.

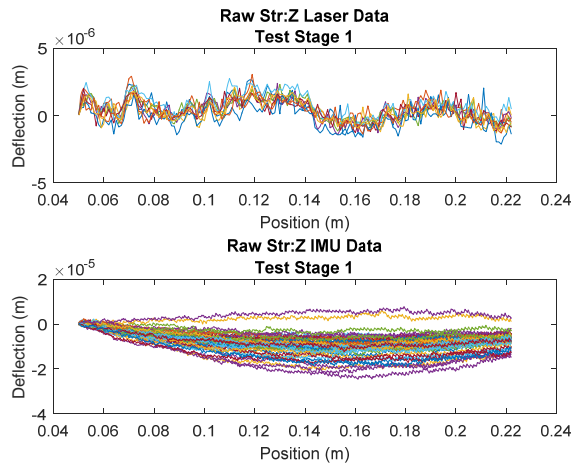


Figure 6. Example uncleaned data.

Each line in the plots represents one of the redundant runs that were performed sequentially, with the assumption that no appreciable change occurs to the condition of the rails during data collection. Each testing cycle collects 10 runs from the laser-based sensor, and 50 from the IMU. The difference in magnitude from these two sets of data occurs due to the IMU having a worse signal to noise ratio, and incidentally, is why the IMU needs more runs to characterize the underlying characteristics.

In Figure 6, the variation between runs for the IMU data is significantly greater than the laser-based data. This is expected as the laser measurement device is a higher fidelity piece of equipment. Nonetheless, the IMU-based results can be cleaned and merged to find the underlying form of the rail deflection path. Figure 7 shows the average deflection values taken during the first test cycle for the translational data in each of the three directions.

Once the data for each test day has been cleaned and consolidated, the next step is to compare each day with the baseline fault-free data collected on the first testing cycle (Stage 1). The analytic amplitude of these residual values can be tracked over time to produce metrics indicating the overall health of the rail.

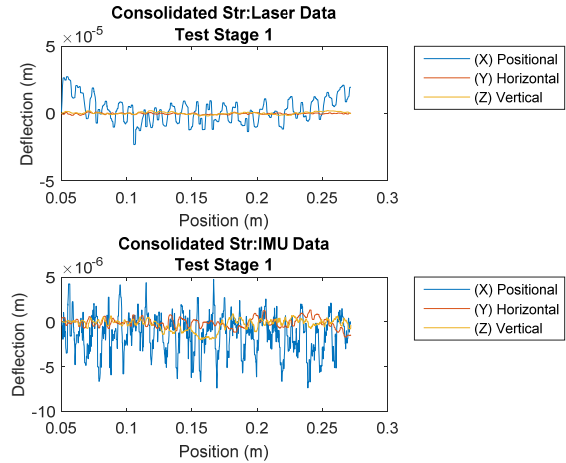


Figure 7. Cleaned and merged data.

Figure 8 shows these error metrics based on rail position for both the high-fidelity laser-based data and IMU-based data for selected test stages. Much can be learned about the quality of the IMU versus that of the laser from these plots. First, notice that the progressive peak centered near the 0.13 m position appears clearly in both sets of data. This corresponds to the front truck encountering the induced degradation. A secondary peak near 0.23 m corresponding to the second truck encountering the degradation can also be seen appearing to a lesser degree in both data sets. This echoing of form from the high-fidelity laser-based data to the IMU-based data confirms that the degradation being captured by the IMU is accurate in form and position.

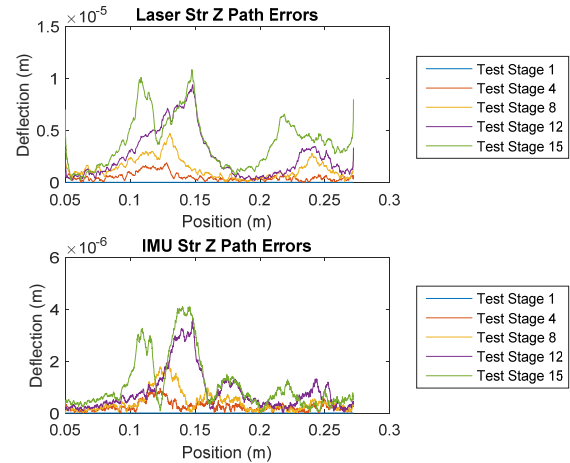


Figure 8. Select position-based straightness error values.

Another important conclusion that can be drawn from these plots is that, although the form and shape of the captured degradation is similar between the two sensors, the magnitudes are significantly different. The amplitudes of the captured degradation from the IMU are roughly two to three times smaller than those from the laser-based system. This

indicates that the sensitivity of the IMU-based method is lower than that of the laser-based system. This result is further corroborated by the difference in the signal-to-noise ratio between the IMU and reference data. Despite this higher noise level and lower sensitivity, the IMU is still able to capture and accurately characterize the induced degradation with a traceable progression similar to that found in the laser data.

Figure 9 shows the progression of the total damage indicated across the rail at each test stage for both the IMU- and reference-based datasets. These charts show the integral of the measured damage in both the vertical and horizontal directions, which are the directions most affected by the induced ‘spalling’. In both instances, Stage 1 is taken as the baseline and therefore by definition has the trivial value of zero.

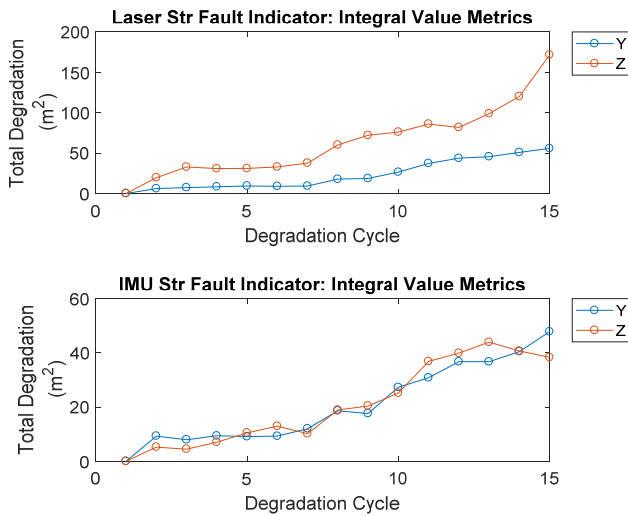


Figure 9. Straightness integral damage progression in directions of interest.

An important point of clarification is that the metrics developed in this work do not directly translate to the physically measurable units of degradation. The layers of processing to produce the metrics obfuscate the direct mapping. In other words, a metric value of 20 m² does not necessarily imply that a hand-made, direct measure of the degradation would also yield a result of 20 m². For example, if both the IMU derived metric and the hand measurements show values of 40 when the laser sensor derived metric shows a value closer to 100, this does not instantly imply that the IMU is more accurate than the laser-based results. Such discrepancies could result because the signal-to-noise ratio is higher in this bandwidth, or because of any number of other artifacts of processing. Nonetheless, and more importantly, the relative progressions and their correlations to the values of degradation manually measured with a handheld micrometer are very good.

The correlation between cumulative damage captured by the IMU- and the laser-based methods is approximately 0.98 for both the Y- and Z- directions, respectively. This confirms statistically that though there are differences in scale, the captured trends are nearly identical. Also important to note, is that the Y- and Z- directions for both the laser- and IMU-based degradation show a correlation above 0.95, both to each other and the handmade direct measurements of the degradation, lending further credibility to the merit and quality of the captured values and trends. A full correlation analysis can be seen in Figure 10.

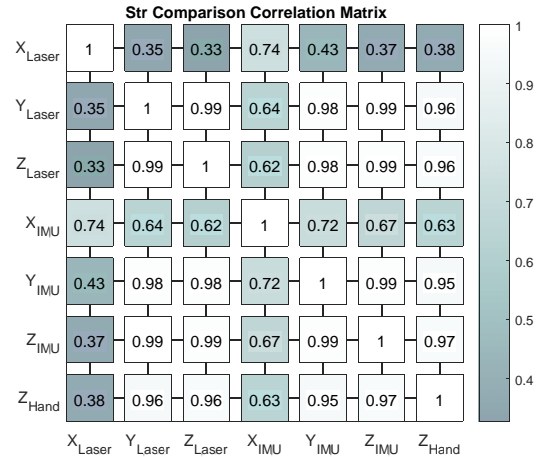


Figure 10. Straightness correlation analysis.

A final interesting note on this analysis is that, even though as expected, both the laser- and IMU-based X-directional errors (positioning error motions) show little correlation to the handmade measurements of cumulative degradation, they do exhibit moderately strong correlations to each other (0.72). This seems to indicate that although the positioning error motion does not capture the induced damage in a significant manner (per Table 2), the positioning error motion is still affected by the subtle changes in the physical system; in this case, specifically in the direction of travel.

Similar to the translational errors captured by the accelerometer, angular errors were captured via the accelerometer and rate gyroscope in the IMU. Shown in Figure 11, the progressive stages of the induced degradation are captured by both the IMU and the laser-based reference system. In Figure 11, it is easy to distinguish the two peaks associated with the two separate rail trucks encountering the degradation as they pass. The angular data is more consistent than the straightness data for lower frequencies, making it easier to analyze for fine details.

The angular integral damage progressions, as shown in Figure 12, are all also highly similar to those found in both the straightness analysis and handmade measurements. Again, the scales and seeming sensitivities are significantly lower in the IMU-based results than those of the high fidelity

laser-based results, but the overall trends are nearly identical. It is important to note here that the relative values of the metrics in each direction are sensitive both to the level of noise in that signal and the size of the filtering window selected for denoising, as described in an earlier section. Steps to mitigate this effect and/or more precisely prescribe the selection of the denoising window are currently under investigation. The more important aspect for this paper is that the resulting trends show strong correlations both between themselves, and to the direct hand-held micrometer measurements, despite the differences in scales.

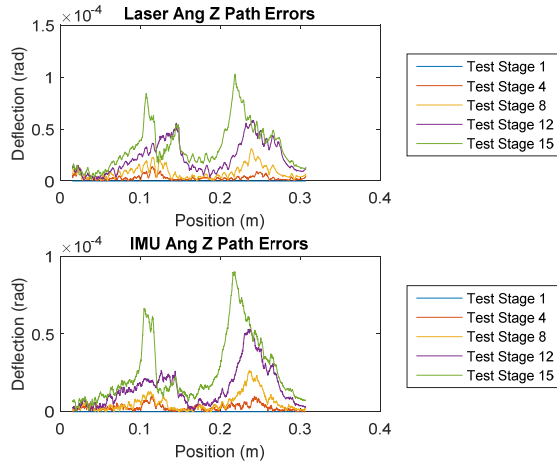


Figure 11. Select position-based angular error values.

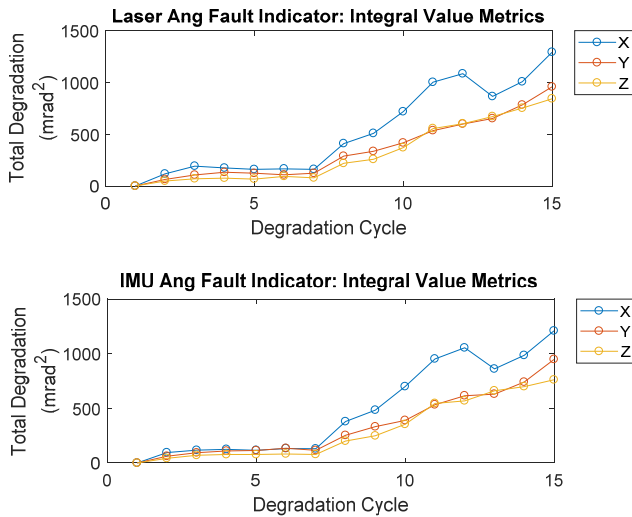


Figure 12. Angular integral damage progression in directions of interest.

Figure 13 shows the correlation analysis of the angular errors along with the manual hand-micrometer depth measurements. From this figure, we can see that the lowest correlation to the independent hand measurements is 0.93, which is a strong correlation. In fact, all the correlations

presented in this analysis are strong enough to suggest that the metrics are all capturing the same underlying cause, in this case, the progression of induced degradation. Such high correlation between independent metrics inferring degradation supports a high confidence in any calculated degradation values reported by an IMU utilizing this diagnostic approach.

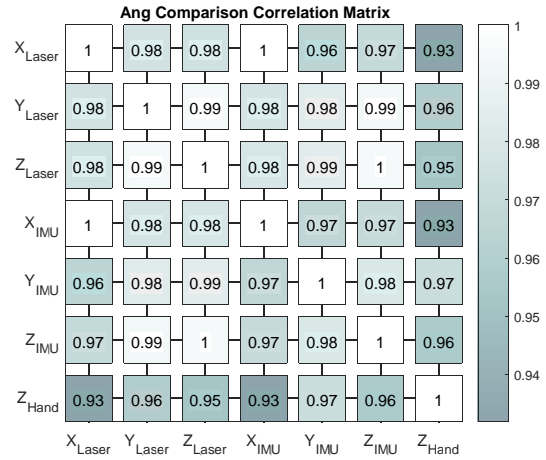


Figure 13. Angular correlation analysis.

6. CONCLUSIONS

An experiment was designed and implemented on a linear axis rail to simulate ‘spalling’ on a common production machine. The purpose of this experiment was to verify the viability of a novel IMU-based sensor system and to develop metrics suitable for capturing and quantifying degradation signatures for diagnostic and prognostic monitoring. High-fidelity laser-based data and handmade measurements of the known degradation were collected and used for verification and validation of the IMU-based results and associated metrics.

Both the IMU-based and laser-based detectable degradation metrics showed strong correlations to one another as well as to the hand-taken values. These strong correlations confirm that the IMU is a viable, accurate, and efficient sensing system that can provide comparable results to the more expensive laser-based system. The analysis further shows that although the accelerometer data from the IMU exhibits a significant low-frequency variance, steps can be taken to mitigate this effect.

Future work will focus on the development of comprehensive methods for identifying and isolating both truck-based defects and rail-based defects. Additional data will be generated in an ongoing effort to verify and validate the IMU-based method and associated metrics as well as to produce standard datasets on which novel diagnostic algorithms can be developed. Ultimately, such algorithms could enable the use of IMU-based methods for diagnostics, prognostics, and

health management of linear axes within production machines.

ACKNOWLEDGEMENTS

The authors thank Brian Pries, Travis Shatzley, Dan Falvey, and Jay Brandenburg of the Fabrication Technology Group at the National Institute of Standards and Technology (NIST) for their outstanding contributions with the experimental setup.

NIST DISCLAIMER

Certain commercial equipment, instruments, or materials are identified in this paper to foster understanding. Such identification does not imply recommendation or endorsement by the National Institute of Standards and Technology, nor does it imply that the materials or equipment identified are necessarily the best available for the purpose.

REFERENCES

- International Organization for Standardization (2012). *ISO 230-1 - test code for machine tools – part 1: Geometric accuracy of machines operating under no-load or quasi-static conditions*.
- InvenSense Incorporated (2016). *MPU-6050 six-axis (gyro + accelerometer) MEMS MotionTracking™ device*: <https://www.invensense.com/products/motion-tracking/6-axis/mpu-6050/>
- Khan, A. W. & Chen, W. (2009). Calibration of CNC milling machine by direct method. *2008 International Conference on Optical Instruments and Technology: Optoelectronic Measurement Technology and Applications* (p. 716010), November 16-19, 2008, Beijing, China. doi: 10.1117/12.807066
- Li, Y., Wang, X., Lin, J., & Shi, S. (2014). A wavelet bicoherence-based quadratic nonlinearity feature for translational axis condition monitoring. *Sensors*, vol. 14(2), pp. 2071-2088.
- Sato, R. & Nagaoka, K. (2011). Motion trajectory measurement of NC machine tools using accelerometers. *International Journal of Automation Technology*, vol. 5(3), pp. 387-394.
- Sato, R., Nagaoka, K., & Sato, T., "Machine motion trajectory measuring device, numerically controlled machine tool, and machine motion trajectory measuring method," USA Patent US9144869 B2, Sep. 29, 2015.
- Smith, K. S. & Hocken, R. J., "Dynamic metrology methods and systems," USA Patent US8401691 B2, Mar. 19, 2013.
- Teti, R., Jemielniak, K., O'Donnell, G., & Dornfeld, D. (2010). Advanced monitoring of machining operations. *CIRP Annals - Manufacturing Technology*, vol. 59(2), pp. 717-739. doi: 10.1016/j.cirp.2010.05.010
- Uhlmann, E., Geisert, C., & Hohwieler, E. (2008). Monitoring of slowly progressing deterioration of

computer numerical control machine axes. *Proceedings of the Institution of Mechanical Engineers, Part B: Journal of Engineering Manufacture*, vol. 222(10), pp. 1213-1219.

- Vogl, G. W., Weiss, B. A., & Donmez, M. A., "A sensor-based method for diagnostics of machine tool linear axes," presented at the Annual Conference of the Prognostics and Health Management Society 2015, Coronado, CA, 2015.
- Vogl, G. W., Donmez, M. A., & Archenti, A. (2016). Diagnostics for geometric performance of machine tool linear axes. *CIRP Annals - Manufacturing Technology*, vol. 65(1), pp. 377-380.
- Zhou, Y., Mei, X., Zhang, Y., Jiang, G., & Sun, N. (2009). Current-based feed axis condition monitoring and fault diagnosis. *4th IEEE Conference on Industrial Electronics and Applications, ICIEA 2009* (pp. 1191-1195), May 25-27, 2009, Xi'an, China. doi: 10.1109/ICIEA.2009.5138390

BIOGRAPHIES



Dr. Gregory W. Vogl is a Mechanical Engineer at the National Institute of Standards and Technology (NIST) located in Gaithersburg, Maryland. He received his B.S. (2000), M.S. (2003), and Ph.D. (2006) degrees in Engineering Mechanics from Virginia Tech, Virginia, USA. Currently,

Greg is a member of the *Prognostics, Health Management, and Controls* (PHMC) project, which seeks to help enable robust real-time diagnostics and prognostics for smart manufacturing systems. Previously, he designed, fabricated, and experimented on microelectromechanical systems as a National Research Council Postdoctoral Researcher at NIST. He then joined the Production Systems Group, in which he worked on machine tool metrology and standards development. His interests include machine tool spindle health, diagnostic and prognostic methods, nonlinear dynamics, engineering mechanics, and metrology.



Dr. Michael E. Sharp is a Reliability Engineer at the National Institute of Standards and Technology (NIST) located in Gaithersburg, MD. He received a B.S (2007), M.S. (2009), and Ph.D. (2012) in Nuclear Engineering from the University of Tennessee, Knoxville, TN, USA. His

research interests include signal analytics, machine learning, artificial intelligence, optimization, and natural language processing. Michael has worked on a wide array of projects including image processing for elemental material recognition, prognostics for electric motors undergoing transient operations, and control systems for deep space reactors. He currently works with the NIST Systems Integration Division for Smart Manufacturing.